Acta Radiologica Oncology 25 (1986) Fasc. 3

FROM THE DEPARTMENT OF RADIATION PHYSICS, KAROLINSKA INSTITUTET AND UNIVERSITY OF STOCKHOLM, S-10401 STOCKHOLM, SWEDEN, AND SECTION OF PHYSICS, DEPARTMENT OF RADIOLOGY, HOSPITAL CLINICO UNIVERSITARIO, E-50009 ZARAGOZA, SPAIN.

DOSIMETRY AND QUALITY SPECIFICATION OF HIGH ENERGY PHOTON BEAMS

A. BRAHME and P. ANDREO

Abstract

A number of quality descriptors are defined characterizing the photon attenuation and lepton contamination properties of high energy photon beams for radiation therapy. The dependence of the quality parameters on the design of the clinical beams such as the incident electron energy, target and filter thicknesses, field size and depth in the phantom are analyzed in some detail using analytical and Monte Carlo techniques. It is shown that the mean attenuation coefficient of the beam for a standard field size of 10 cm × 10 cm is related very accurately to the mean stopping power ratio for ionizing chamber dosimetry but also approximately to the equilibrium absorbed dose in the beam for a given photon energy fluence. This means that accurate photon dosimetry can be performed without knowing the acceleration potential, target design or filter thickness for the beam in use. Furthermore, the mechanism behind beam hardening and softening in the phantom are quantitized and suitable quality parameters for the lepton contamination are identified. The latter allow a determination of the lepton contamination for correction of the stopping power ratio near the surface if the contamination is large.

Key words: Dosimetry; photons, quality specification, beam hardening, beam softening, Monte Carlo.

Ionization chamber dosimetry in high energy photon beams is generally simpler than in electron beams due to the smaller beam quality dependence of the stopping power ratio. Over the clinically useful depth interval the stopping power ratio varies only about 5 per cent in 2 to 25 MV photon beams whereas it varies about 15 per cent in 2 to 25 MeV electron beams. Despite this fact photon beam dosimetry suffers from uncertainties of the order of 1 to 2 per cent due the lack of relevant beam quality descriptors characterizing the dosimetric properties of the beam.

Today it is well-known that the photon spectrum is not sufficiently well described for dosimetric purposes by the peak photon energy which generally is quite close to the most probable energy of the electrons incident on the bremsstrahlung target. This fact is mainly due to the significant filtration of the initial bremsstrahlung spectrum by the flattening filter, particularly at high photon energies.

In addition to uncertainties in the definition of the shape of the photon spectrum, the sometimes considerable electron contamination of the photon beam will contribute to the uncertainty in absorbed dose in the build-up and plateau region of the depth dose curve. The electron contamination from the treatment head and the air will generally have a lower stopping power ratio than the complete electron slowing down spectrum in the medium. This is due to the considerable filtering of the low energy electron contamination by multiple Coulomb scattering in the intervening air (11, 31).

The aim of the present investigation is to use the Monte Carlo method to find suitable quality parameters for photon beams allowing a high dosimetric accuracy through a more precise choice of the relevant stopping power ratios. The theoretical background, together with some results mainly for monoenergetic photon beams, will be presented here. Practical stopping power data for dosimetry of clinical bremsstrahlung beams are treated in more detail by ANDREO & BRAHME (6).

Photon transport code

The Monte Carlo code used to simulate the transport of photons in water has been previously described (2, 3). It considers the whole electromagnetic cascade up to a maximum energy of 50 MeV using a direct simulation of the photon interactions and a mixed procedure or Class II scheme (8) for the electrons. The latter scheme was recently included in a modified form (5).

The cascade originated by primary monoenergetic photons or by a bremsstrahlung spectrum, considers the pho-

Accepted for publication 3 February 1986.

ton interactions by direct sampling of individual photoelectric absorption, Compton scattering and pair-producing interactions, until the photon energy goes below the Monte Carlo photon cut-off $T_{c,\gamma}$, chosen between 10 keV and 50 keV for incident photon energies in the range 0.1 to 50 MeV. All generations of electrons and positrons (treated as if they were electrons except for their annihilation at rest) produced through these events are simulated according to a classification of their interactions in catastrophic and non-catastrophic collisions. The first type corresponds to certain events in which the energy or the deflection angle is changed by more than a predetermined value, and includes inelastic electron-electron collisions where the energy loss is greater than a cut-off energy, Δ, elastic nuclear collisions where the scattering angle is greater than a cut-off angle, δ, and all bremsstrahlung interactions. In the segment between those major events, non-catastrophic collisions account for small electron energy losses, calculated by the restricted stopping power, and multiple scattering restricted to angles less than δ, calculated according to ANDREO & BRAHME (5) using a Gaussian angular spreas based on a restricted mass scattering power. For the present purposes, restricted energy loss straggling has not been considered as it was shown that its influence is minimal for the low cut-off energies, Δ, commonly employed for the inelastic collisions.

The transport of electrons is simulated until their energy goes below the Monte Carlo electron cut-off, $T_{c,e}$, determined as a function of the thickness of the layers in which the absorbing medium is divided to compute the different physical quantities of interest (energy absorption, energy and angular spectra, etc). The electron energy cut-off, $T_{c,e}$, is chosen in such a way that the corresponding c.s.d.a. range at the maximum electron energy, r_0, equals half of the thickness of the layer, with a maximum limiting value of 500 keV for the highest energies when the primary photons are monoenergetic. If the simulation of a bremsstrahlung spectrum is considered, then $T_{c,e}$ is decreased to account for the low energy component of the spectrum if such a low component contains photons of less than 500 keV.

Of special interest for this work is the calculation of the depth variation of energy deposition and electron spectra differential in energy. These two distributions will enable the determination of the dependence of the stopping power ratio on the photon beam quality. The Monte Carlo code used here computes the energy deposition for point monodirectional beams as a function of radius and depth, $D_{pm}(z,r)$. This allows the calculation of central axis depth dose distribution for plane parallel beams (D_{pp}) of different radii R according to

$$D_{pp}(z,R) = \int_0^R D_{pm}(z,r) \quad 2\pi r dr \tag{1}$$

Electron spectra $\Phi_E(z)$ including delta rays (i.e., total slowing down spectra) are determined as a function of depth for broad beams by scoring the electron track lengths per unit volume at each depth z. Energies below the Monte Carlo cut-off $T_{c,e}$ are taken into account by the scheme described by NAHUM (30), using the c.s.d.a. approximation.

Bremsstrahlung spectra

A limited amount of experimental data has been published on bremsstrahlung spectra produced by clinical accelerators (7, 15, 16, 23, 24) and non-clinical machines (cf. 20). Furthermore these authors do not agree on the necessary corrections that have to be performed on the basic experimental data. In a few cases calculated spectra are also available for the same configuration (26, 34). The lack of consistent experimental bremsstrahlung spectra covering the energy range of interest for the present Monte Carlo simulation has encouraged the use of calculated spectra for the majority of the results in the present work. Fortunately the exact spectral shape has a rather small influence on the stopping power ratio when it is related to the attenuation properties of the beam and not to the acceleration potential (cf. ref. 6 and Figs 2 and 3).

Despite its wide use also at low energies, it is well-known that the SCHIFF (39) cross section is valid for high energies only ($E,k>>mc^2$). Consequently we have relied upon the whole bremsstrahlung cross section package given by KOCH & MOTZ (20) for the calculation of thick target bremsstrahlung spectra. An existing typographical error in Table V of the KOCH & MOTZ work (cf. 25) has been accounted for.

In the case of thick targets, the photon spectrum, i.e. the number of photons per MeV interval, from a target with thickness t can be calculated from (cf. 43).

$$\Phi_k(E_0,t) = \int_0^t e^{-\mu(t-z)} dz \quad \int_k^{E_0} \Phi_E(E_0,z) \frac{d\sigma(E,k)}{dk} dE \tag{2}$$

where Φ_E is normalized according to

$$\int_k^{E_0} \Phi_E(E_0,z)\, dE = 1 \tag{3}$$

and

E_0 = incident electron energy
k = photon energy
$\Phi_E(E_0,z)$ = electron spectrum, differential in energy, at depth z produced by electron with a monoenergetic incident energy E_0
μ = attenuation coefficient of the target for photons of energy k
$\sigma(E,k)$ = bremsstrahlung cross section for an electron with energy E and photons with energy k.

An exact knowledge of the electron spectrum Φ_E would require a Monte Carlo simulation of its own as the ap-

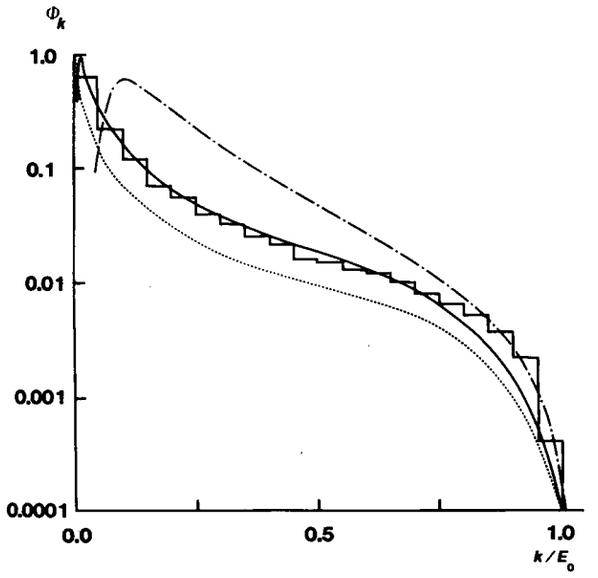

Fig. 1. Bremsstrahlung spectra of 2 (—·—), 20 (—) and 50 (· · ·) MeV electrons incident on 1 mm of tungsten obtained with the approximation given in eq. (4). The histogram corresponds to a Monte Carlo calculation on 1 mm Ta done by ROGERS & BIELAJEW (37).

proximate expression given by TSAI (43) is valid for ultra high energies. Such a simulation is out of the scope of the present work. We have instead approximated the above formula by the expression

$$\Phi_k(E_0, t) = \int_0^t e^{-\mu(t-z)} \frac{d\sigma(\bar{E}_z, k)}{dk} dz \qquad (4)$$

i.e., the cross sections are evaluated at the mean energy of the primary electron spectrum at depth z, given by (4, 10, 33)

$$\bar{E}_z = E_0 \frac{S_{tot} \exp(-zS_{rad}/E_0) - S_{col}}{S_{rad}} \qquad (5)$$

Results produced by such an approximation are shown in Fig. 1, where the bremsstrahlung spectra produced by electrons of 2, 20 and 50 MeV incident on a tungsten target of thickness equal to 1 mm calculated using eq. (4) are plotted as a function of k/E_0. Results of ROGERS & BIELAJEW (37) for a target of 1 mm of tantalum calculated by the Monte Carlo method have been included for comparison. The agreement is good enough for the present purposes, although there exists a certain softening of the spectrum partly due to the different densities of W and Ta and the neglection of multiple scattering of the electrons in the target using eq. (4). Differences in the spectral shape at 2 and 50 MeV are explained in terms of the thickness of the target, that can be considered as thick for the low energy while it is thin for the highest energy.

The calculated spectra have been used as input to the present Monte Carlo code. Due to the difference of several orders of magnitude existing in most of the photon fluence spectra (see for instance Fig. 1), the simulation of the spectrum requires very large computation times in order to get results statistically significant for the high energy component of the spectrum. In the present work a direct Monte Carlo simulation of the entire photon spectrum has been performed using 100 equally distributed energy intervals.

Factors affecting photon beam quality

A photon beam is completely characterized by the photon fluence differential in energy and angle, but it needs generally further description with regard to unavoidable contaminations, for example by secondary photons, electrons, positrons and neutrons. As the neutrons generally give a negligible dose contribution they will not be discussed further here.

Most bremsstrahlung beams originates from a fairly small effective radiation source due to a narrow initial electron beam and a small influence of photon scatter in flattening filters. This means that the angular distribution of photons is approximately that from a point isotropic source placed close to the target. At least at acceleration potentials above a few MeV the photon scatter in the treatment head have a minor influence on the total photon fluence (32).

All photon beams are to some extent contaminated by leptons (in the present context electrons and positrons) generally produced by photoelectric, compton and pair producing interactions in the materials traversed by the beam. This charged particle contamination has generally a considerable influence on the shape of the photon depth dose curve in the build-up region. In particular the relative surface dose and the depth of dose maximum is determined by the amount of charged particle contamination. The location of the principal contamination sources varies considerably with photon beam energy.

At low photon energies (<10 MV) the air volume between source and patient is the main contributor of secondary electrons because the electron energy and range is low and their scattering power high. Electrons from the treatment head will therefore not reach the patient principally because they are scattered out of the beam by the air (scatter filtering). The last few decimeters of air in front of the patient will therefore generally be the main electron source.

At high photon energies (>20 MV) on the other hand, the last thick material layer in the beam, usually the flattening filter, will be the main electron and positron contamination source. This is so since, in this energy range, the electrons are more forward directed, their energy is high and their scattering power low. At the same time the electron range in air is very long so the air

contribution will be very far from saturated and thus quite small. The forward directed high energy lepton contamination from the treatment head is therefore the major contamination source of high energy photon beams and has generally a very significant influence on the depth of dose maximum and the relative surface dose (9, 29, 35).

The lepton contamination has therefore a dominant effect on the shape of the depth dose curve at high photon beam energies as illustrated in Fig. 2 for a 50 MV beam. The dotted line is the depth dose in a uniform beam of 10 cm × 10 cm cross section at SSD 100 cm. The solid line is the resultant depth dose when a large fraction of the photon generated lepton contamination from the down stream end of the carbon electron stopper is removed by a purging magnet (magnetic field line integral $=\int B\mathrm{d}l \approx 1$ T cm) placed close to the target. It is seen that the depth of dose maximum is increased from 4 to 7 cm by the purging magnet. The depth dose of the removed lepton contamination is illustrated by the solid line obtained by substracting the depth dose curve with purging magnet from that without (cf. similar results in ref. 29). The depth dose of a pure photon beam as calculated by the present Monte Carlo code is also included for comparison. It is clear that most of the electron contamination was removed by the magnet. It is a fortuitous effect that in the energy range around 15 MV the lepton contamination has a minimum and high quality photon beams can easily be produced without electron filter or purging magnet.

When the lepton contamination is as high as in Fig. 2, the difference in stopping power value for the photon and lepton dose fractions can cause an appreciable dosimetric uncertainty in the build-up region. At lower photon energies similar differences in depth dose are seen (cf. e.g. 22) but the differences in stopping power of the electrons are smaller due to the slight influence of the density effect with a reduced dosimetric uncertainty as result.

The shape of the bremsstrahlung spectrum as determined by the target and the flattening filter has also a certain influence on the shape of the resultant depth dose curve (14). In general a thin target or a target with a low atomic number electron stopper will generate a harder bremsstrahlung spectrum (36). Similarly will a low atomic number flattening filter harden the beam whereas high atomic number filters soften it at high bremsstrahlung energies and harden it at low energies. It should be pointed out in this context that the last mentioned reference overemphasizes the influence of the shape of the bremsstrahlung spectrum on the shape of the depth dose curve, as the lepton contamination was not specifically considered. For example will a lead filter produce a larger lepton contamination than an aluminium filter in broad photon beams (31). This explains about half the improvement of the depth dose obtained by using an aluminium filter (cf. 36).

Another important quality dependence in clinical photon beams are the variations across the beam. Today it is

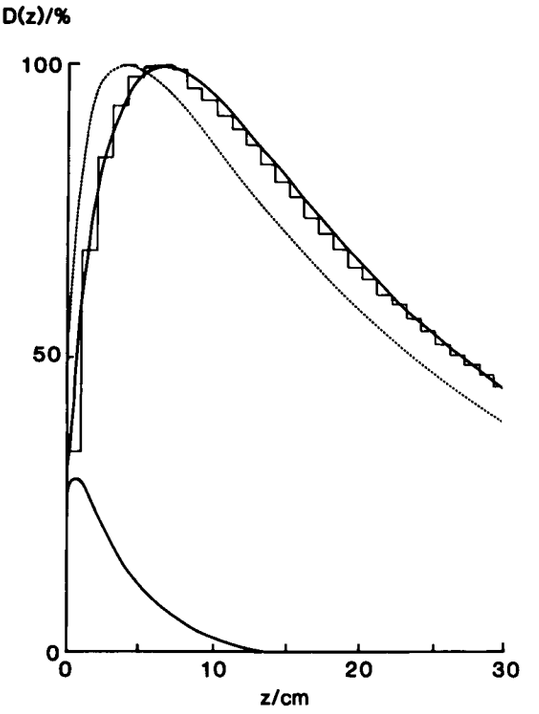

Fig. 2. Central axis depth dose distribution for 50 MV photon beams. The dotted curve pertains to a 10 cm by 10 cm^2 field size and the solid line to the same field but with a purging magnet to remove the electron contamination generated by the bremsstrahlung beam in the electron stopper consisting of 15 cm of graphite. The solid histogram corresponds to a 0.2 r_0 thick tungsten target as calculated by the present Monte Carlo code. The slightly larger penetration of the experimental beam with purging magnet is at least partly due to the beam hardening in the electron stopper.

well known that the spectrum from a bremsstrahlung target varies with the angle of emission (cf. e.g. 12, 13). This effect is quite small in low energy beams whereas it is substantial in high energy beams, specially if a low atomic filter is used for beam flattening. By using a suitably designed flattening filter including materials of a high atomic number, which soften the beam on the central axis, this variation can be considerably reduced or even eliminated. In the present work this variation is therefore neglected and all calculated photon spectra are averaged over all emission angles. However, the quality variation across the beam in the phantom, due to variation of the Compton scattered dose contribution, is taken fully into account (cf. 32).

The above factors taken together imply that the acceleration potential of a bremsstrahlung beam is a very poor descriptor of the dosimetric properties of the beam (cf. also 30). New characteristics of high energy photon beams are therefore needed to allow accurate dosimetry.

Quality specification

Background

Traditionally the radiation quality of a photon beam is specified by the acceleration potential in kilovolt (kV) for conventional roentgen rays and megavolt (MV) for high energy bremsstrahlung beams. From the previous discussion it is clear that this information is not sufficient to specify the beam quality for dosimetric purposes. For conventional roentgen rays the half value layer or depth (HVD) is often used as an additional quality descriptor and has recently been proposed for use also at higher photon energies (19). This is a better descriptor of the dosimetric properties of a photon beam, but as can be seen from Fig. 2 this depth is considerably influenced by the lepton contamination of the beam. Therefore it cannot be used to choose an appropriate stopping power value.

NACP (27) proposed to use the ratio of the absorbed doses at two depths as a measure of radiation quality. Several dosimetry protocols are available today in which the specification of the quality of a photon beam is based on the dose or ionization ratio at two different depths (1, 28, 40). These ratios are by far better descriptors of the dosimetric properties of a bremsstrahlung beam.

Theory

The value of using the 10 to 20 cm depth dose ratio is its close relation to the practical attenuation coefficient, μ_p (cf. 13, 17), through the simple equation

$$\mu_p = k \ln \left[\frac{D_{10}}{D_{20}} \right] \tag{6}$$

where $k=10\ \mathrm{m}^{-1}$. Naturally this expression (and eq. 11) assumes that the depth of transient equilibrium is less than 10 cm below the surface so the 10 and 20 points are on the quasi-exponential fall-off portion of the depth dose curve. If instead of the dose ratio the ionization ratio is used it should strictly be multiplied by the appropriate stopping power ratio since

$$\frac{D_{10}}{D_{20}} = \frac{J_{10}}{J_{20}} \cdot \frac{s_{w,a,10}}{s_{w,a,20}} \tag{7}$$

Therefore, only if the stopping power is sufficiently depth independent the ionization ratio could be used instead of the dose ratio (6, 42).

The practical attenuation coefficient accounts beside the pure photon absorption also for the inverse square attenuation of a beam from a finite radiation source. The mean attenuation coefficient, $\bar{\mu}$, of the photon spectrum at hand can therefore be calculated by an inverse square correction on μ_p. However, owing to the approximate exponentiality of the inverse square correction as seen from the following relation

$$e^{-\bar{\mu}z}\left(1+\frac{z}{f}\right)^{-2} = e^{-(\bar{\mu}+2/f)z} + \left(\frac{z}{f}\right)^2 + o\left(\left(\frac{z}{f}\right)^3\right) \approx e^{-\mu_p z} \tag{8}$$

where f is the distance from the point source to the point where μ_p was measured. Thus the following simple relation between $\bar{\mu}$ and μ_p holds

$$\bar{\mu} = \mu_p - m \tag{9}$$

and m may thus be approximated by

$$m = \frac{2}{s_{vir} + \bar{z}} \tag{10}$$

where s_{vir} is the distance from the virtual point source to the phantom surface and $\bar{z}$ is the mean depth of measurement when determining μ_p (cf. 13, 38). For the most common radiation geometry in radiation therapy, s_{vir} is 100 cm and $\bar{z}$ is 15 cm, assuming the D_{10}/D_{20} ratio is being used to determine μ_p, the correction for the finite source to surface distance is of the order of $m=1.74\ \mathrm{m}^{-1}$. Within about 10 cm from $\bar{z}$ this value gives dose errors less than one per cent according to eq. (9). Alternatively $\bar{\mu}$ can be determined from the tissue phantom ratio TPR_{10}/TPR_{20} using an equation similar to eq. (6)

$$\bar{\mu} = k \ln \left(TPR_{20}^{10} \right) \tag{11}$$

The dose or *TPR* ratios thus allow a determination of the mean attenuation coefficient of the photon beam. Furthermore $\bar{\mu}$ and μ_{en} are approximately proportional at photon energies above a few MeV as seen from Fig. 3. Monte Carlo calculated $\bar{\mu}$ values for monoenergetic photon beams are plotted here as a function of energy for a few different field sizes. μ and μ_{en} data from HUBBLE (18) are also included for comparison. The agreement of the calculated values for very small field sizes ($\bar{\mu}_0$) with tabulated narrow beam attenuation coefficients (μ) is very good and demonstrates the consistency of the present Monte Carlo code. The difference between the mean attenuation coefficient in broad beams, ($\bar{\mu}_\infty$) and the energy absorption coefficient (μ_{en}) is quite small above a few MeV but increases with decreasing photon energy. The increasing differences at low energies are due to the increasing influence of multiple photon scatter and the quasilocal absorption of scattered photons that are not included in the determination of μ_{en}.

This implies that the equilibrium absorbed dose in high energy photon beams, as given by (cf. 42)

$$D_{eq} = \frac{-1}{\varrho} \operatorname{div} \vec{\Psi} = \int \Psi_E \frac{\mu_{en}(E)}{\varrho} dE = \Psi \cdot \frac{\bar{\mu}_{en}}{\varrho} \tag{12}$$

where

$$\bar{\mu}_{en} = \frac{\int \Psi_E \mu_{en}(E)\, dE}{\int \Psi_E\, dE} \tag{13}$$

is also well related to the mean attenuation coefficient $\bar{\mu}$ of the beam. The mean attenuation coefficient $\bar{\mu}$ as deter-

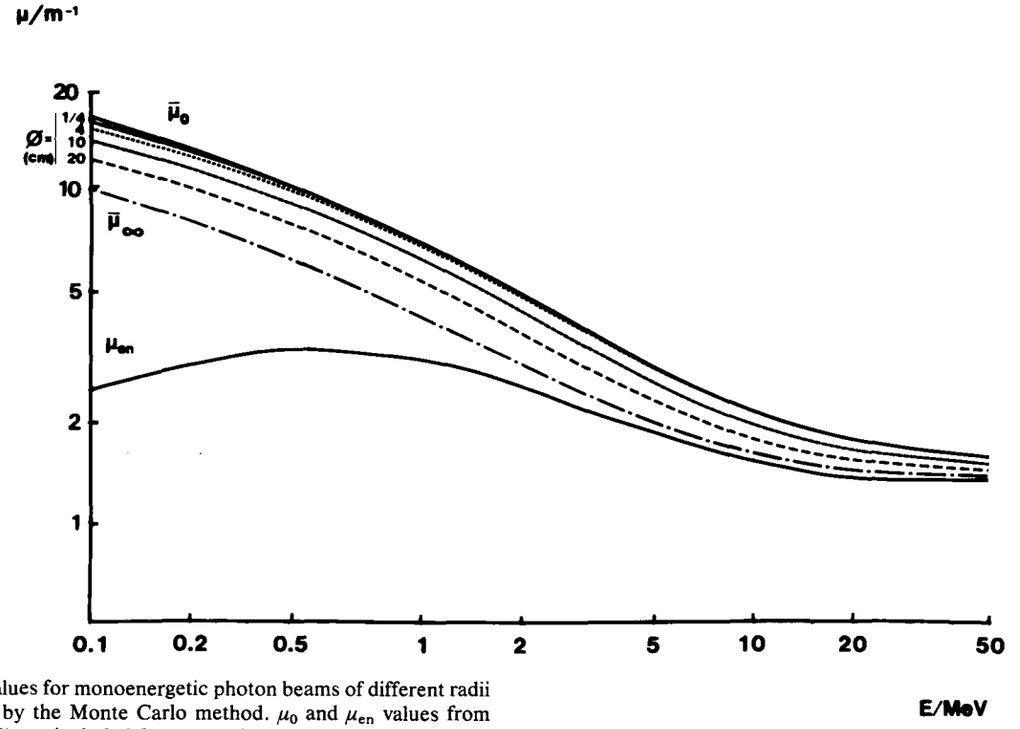

Fig. 3. $\bar{\mu}$ values for monoenergetic photon beams of different radii calculated by the Monte Carlo method. μ_0 and μ_{en} values from HUBBLE (18) are included for comparison.

mined by eqs (6)–(11) should therefore be a very practical descriptor for dosimetry of photon beams. In low megavoltage photon beams where the discrepancies between $\bar{\mu}$ and μ_{en} are larger $\bar{\mu}$ is still a rather good descriptor due to the small variation of the stopping power ratio at low to subrelativistic energies where the influence of the density effect is minimal.

Beam hardening

Due to the close proportionality between kerma, absorbed dose and energy fluence beyond the depth of dose maximum (42) the depth dependence of $\bar{\mu}$ can be determined from the depth dependence of the energy fluence Ψ. When $\bar{\mu}$ is determined through eqs (6)–(11) a mean value is obtained that pertains to a certain depth interval. This mean value can be derived from the depth dependence of the energy fluence according to the equation

$$\Psi(z) = \int \Psi_E(0)\, e^{-\mu(E)z} dE = \Psi(0)\, e^{-\bar{\mu}z} \tag{14}$$

or

$$\bar{\mu}(z) = \frac{-1}{z} \ln \left\{ \frac{\int \Psi_E(0)\, e^{-\mu(E)z} dE}{\int \Psi_E(0)\, dE} \right\} \tag{15}$$

This latter expression can be considerably simplified by expanding it in a power series of μz, keeping the first two terms

$$\bar{\mu}(z) = \bar{\mu} - \frac{z}{2}\sigma_\mu^2 \tag{16}$$

where

$$\bar{\mu} = \frac{\int \Psi_E(0)\, \mu(E)\, dE}{\int \Psi_E(0)\, dE} \tag{17}$$

is the mean attenuation coefficient at the surface and

$$\sigma_\mu^2 = \frac{\int \Psi_E(0)\, (\mu(E) - \bar{\mu})^2 dE}{\int \Psi_E(0)\, dE} \tag{18}$$

is the variance of $\mu(E)$. Because the variance of μ by definition always has a positive value the mean attenuation coefficient of the primary photons is an always decreasing function of depth as should be expected due to the beam hardening effect. According to the mean value theorem there is always one point in the interval 0 to z where the true mean value is exactly equal to that given

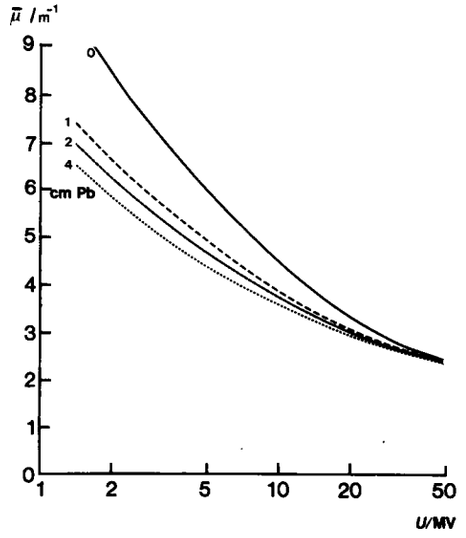

Fig. 4. The mean attenuation coefficient of the photons at the phantom surface for 0, 1, 2 and 4 cm thick lead filters as a function of the electron energy incident on a 0.3 r_0 thick high atomic number target.

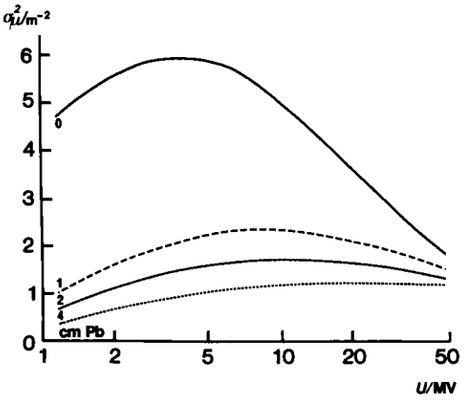

Fig. 5. The variance of the attenuation coefficient of the photons at the phantom surface for 0, 1, 2 and 4 cm thick lead filters as a function of the electron energy incident on a 0.3 r_0 thick high atomic number target.

by eqs (15) and (16). Thus eqs (8) and (11) give a value that is characteristic for some point in the interval 10 to 20 cm.

When σ^2_μ has a small value the depth variation of μ is small an its depth dependence can often be neglected. As seen from eq. (18) σ^2_μ depends both on the shape of the photon spectrum and the energy variation of μ within that spectrum. The μ value variance, σ^2_μ, is therefore a measure of how rapidly the primary beam quality is changing with the depth in the medium since $d\mu/dz=\frac{1}{2}\sigma^2_\mu$. Typical broad beam $\bar{\mu}_o$ and σ^2_μ values are shown in Figs 4 and 5, respectively, for various acceleration potentials (U/MV) and lead filter thicknesses (t/cm) considering an intermediate thickness target ($t=r_0/3$) of high atomic number.

Beam softening

Beside the beam hardening effect on the spectrum of primary photons a photon beam is also influenced by a beam softening effect due to a continuous production of lower energy scattered photons as seen in Fig. 6. The energy deposition in a semi-infinite plane parallel 10 MeV monoenergetic photon beam in water is plotted as a function of the penetration depth. To illustrate the influence of the scattered photons, in addition to the total energy deposition both the energy deposition neglecting just the scattered Compton photons and that neglecting all types of secondary photons are also included. It is seen that most of the secondary photons are generated in Compton interactions and only a minor contribution is due to other secondaries such as bremsstrahlung and annihilation photons (difference between dotted and dashed lines).

The build-up of the secondaries and higher order photons in a broad beam can be well described by a simple analytical model (similar e.g. to that for the build-up of the fluence of secondary electrons, cf. eq. 22) as they are generated in proportion to the primary photon fluence and are absorbed quasi-exponentially with some characteristic mean attenuation coefficient, $\bar{\sigma}$. If $\bar{\mu}_0$ is the mean attenuation coefficient of the primaries and $\bar{\sigma}_0$ is the mean cross-section for production of secondaries, the depth dependence of the energy deposition due to secondaries D_s could be approximated by folding their absorption curve with their production density

$$D_s(z) = K_{col}\beta\frac{\bar{\sigma}_0}{\bar{\mu}_0}\int_0^z \bar{\mu}_0 e^{\bar{\mu}_0 u} e^{-\bar{\sigma}(z-u)} du \qquad (19)$$

where K_{col} is the collision kerma at the surface and β is the ratio of the absorbed dose and the collision kerma beyond the transient equilibrium depth.

After performing the integration this reduces to

$$D_s(z) = K_{col}\beta\frac{\bar{\sigma}_0}{\bar{\sigma}-\bar{\mu}_0}(e^{-\bar{\mu}_0 z}-e^{-\bar{\sigma}z}) \qquad (20)$$

This equation is plotted as the lower dashed line in Fig. 6 whereas the Monte Carlo results are represented by the lower solid line. The agreement is quite good over the first 20–25 cm depth range. At larger depth the high energy small angle scattered Compton photons start to accumulate more significantly and a single attenuation coefficient of the secondaries is clearly a too crude approximation. It is also interesting to note that $\bar{\mu}_0$, the attenuation coefficient of the primaries, is precisely the attenuation coefficient of a narrow photon beam whereas that of both primaries and all secondaries by definition is $\bar{\mu}$ (see Fig. 3). By adding the dose due to primaries to eq. (20), and for

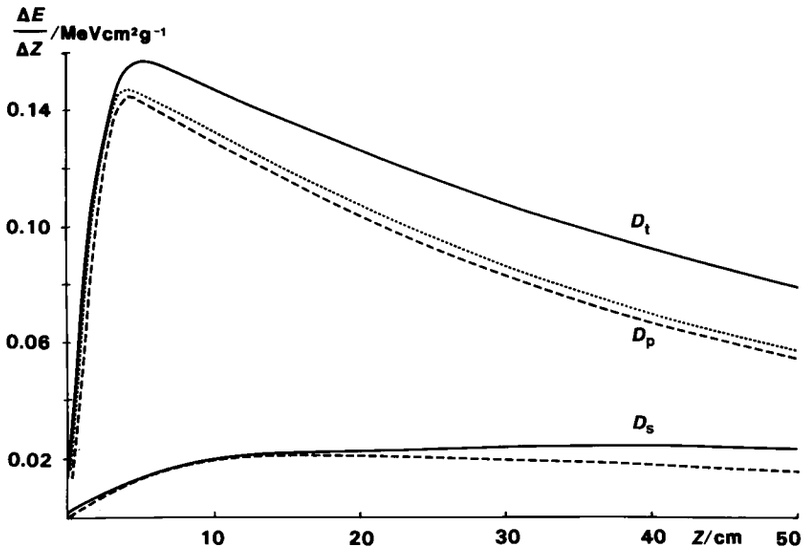

Fig. 6. Depth dose distributions calculated by the Monte Carlo method for a semi-infinite 10 MeV monoenergetic photon beam of plane parallel incidence on water. The absorbed dose has been separated in its primary, secondary and total contributions. The lower dashed line is the contribution of secondaries calculated by a simple analytical model (eq. 20).

simplicity neglecting the transport of secondary electrons, an expression for $\bar{\mu}$ can be obtained since.

$$\frac{D_t}{K_{col}\beta} = e^{-\bar{\mu}_0 z} + \frac{\bar{\sigma}_0}{\bar{\sigma}-\bar{\mu}_0}\left(e^{-\bar{\mu}_0 z} - e^{-\bar{\sigma} z}\right) \approx 1-(\bar{\mu}_0-\bar{\sigma}_0)\,z \ldots \tag{21}$$

Thus $\bar{\mu}_\infty$ is smaller than $\bar{\mu}_0$ by precisely the amount $\bar{\sigma}_0$ over the first attenuation length $1/\bar{\mu}_0$.

Near the surface the effective attenuation coefficient is thus $\bar{\mu}_\infty$ whereas at large depths the lower energy secondaries are completely built up and the attenuation coefficient slowly increases towards the narrow beam value $\bar{\mu}_0$ as seen from the first half of eq. (21) because $\bar{\sigma}$ is generally much larger than $\bar{\mu}_0$ so the last exponential decays most rapidly.

For monoenergetic photon beams as well as for both thin and thick target bremsstrahlung spectra the beam softening effect is generally the dominating factor influencing the shape of the depth dose curve in broad beams over the first few attenuation lengths. This means that the deeper a dose ratio between two points 10 cm apart is measured in a phantom, the higher the ratio will be provided both points are located beyond the depth of transient equilibrium (cf. data in Table 2 in ref. 13). The beam hardening may become more important at very large depths or in high energy beams with a substantial low energy contamination giving a high $\sigma_{\bar{\mu}}^2$ value (see eq. 16).

Lepton contamination

As discussed in the section on factors affecting photon beam quality the lepton contaminations is of major importance for determining the depth of dose maximum but also of the 50 per cent depth dose (see Fig. 2). To get a good description of the shape of the depth dose curve in general at least three independent parameters are needed. Beside μ_p, the practical attenuation coefficient of the photons, two parameters characterizing the electron contamination are needed. The relative amount of contaminating electrons is given by 1-ν and the absorption coefficient of the electrons is specified by μ_e.

Using these three parameters the depth dose of a photon beam can be fitted, with a precision generally much better than one per cent and a correlation coefficient larger than 0.99, by an expression of the type

$$D(z) \propto e^{-\mu_p z} - \nu e^{-\mu_e z} \tag{22}$$

For further details see BRAHME & SVENSSON (13). It is straightforward to show that the depth of dose maximum is given by

$$R_{100} = \frac{\ln\left(\nu\frac{\mu_e}{\mu_p}\right)}{\mu_e-\mu_p} \tag{23}$$

and that the 50 per cent depth dose is given by

$$R_{50} = R_{100} + \frac{\ln\left(\frac{2\mu_e}{\mu_e-\mu_p}\right)}{\mu_p} \tag{24}$$

and generally with sufficient accuracy by simply

$$R_{50} \approx R_{100} + \frac{\ln 2}{\mu_p} + \frac{1}{\mu_e} \tag{25}$$

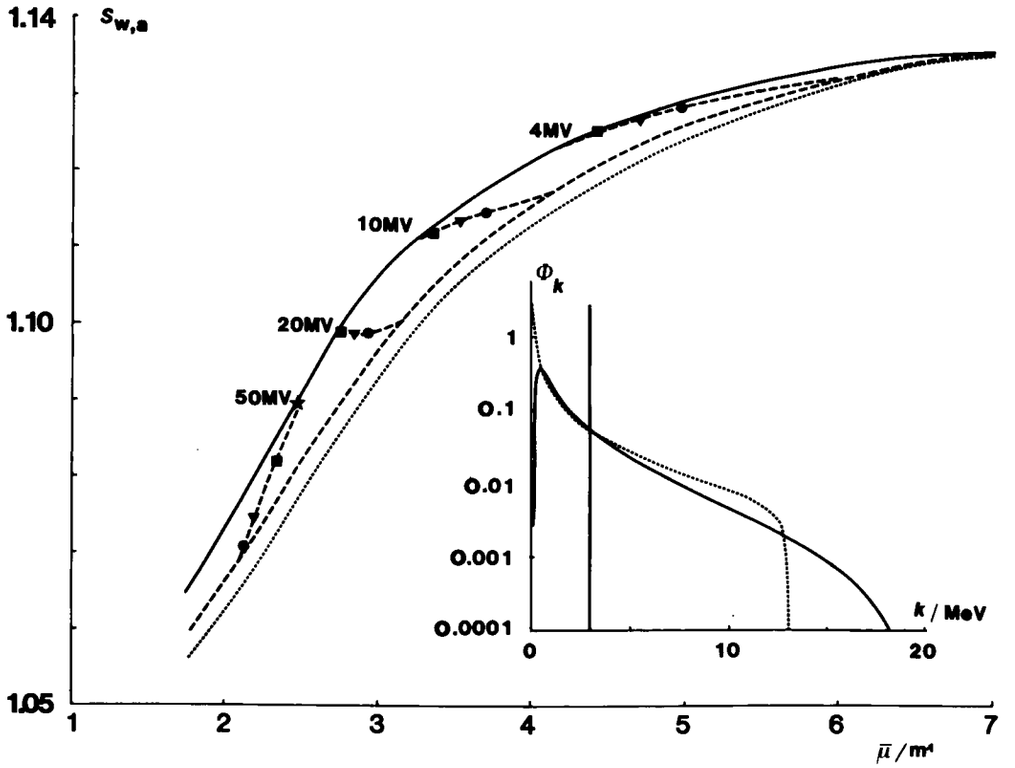

Fig. 7. Spencer-Attix water/air stopping power ratios (I_w=75.0 eV, I_{air}=85.7 eV), density effect according to STERNHEIMER & PEIERLS (41) as a function of $\bar{\mu}$ for monoenergetic photons (—) and bremsstrahlung spectra from thin (. . .) and thick (- - -) tungsten targets. Data for a target of intermediate thickness ($r_0/3$) and varying lead filter thicknesses (circle, triangle, square and star correspond to 1, 2, 4 and 8 cm Pb, respectively) are also included at a few acceleration potentials. The inserted photon spectra pertain to three different types of beams all having the same attenuation coefficient but slightly different stopping power ratios as discussed in the text.

These expressions show that both the half value depth and the depth of dose maximum depend in the same way on the amount of electron contamination as expressed by the parameter ν.

From these equations μ_e can be determined when R_{50}, R_{100} and μ_p are known (eqs 24 or 25) or by dose measurements in the build-up region (13). The amount of electron contamination can now be determined from eq. (23) using

$$\nu = \frac{\mu_p}{\mu_e} e^{R_{100}(\mu_e - \mu_p)} \tag{26}$$

If ν is larger than 0.8, that is less than 20 per cent electron contamination, the influence on the stopping power ratio of the electron contamination in the build-up region should be quite small beyond the first few millimeters near the surface (6). In this context it is interesting that eq. (23) may also be used to determine the depth of dose maximum in a pure uncontaminated photon beam by simply setting ν indentical to unity. It is thus only the attenuation coefficients μ_e and μ_p that determine the depth of dose maximum in well designed photon beams using purging magnets and helium atmosphere in the treatment head (cf. 31).

$\bar{\mu}$ as a quality characteristic for dosimetry

Both energy deposition and electron slowing down spectra have been calculated for monoenergetic photon beams as well as for thin and thick target bremsstrahlung beams in the energy range between 0.1 and 50 MeV using the present Monte Carlo code. Central axis depth dose distributions for plane parallel beams of different radii have been determined. The exponential portion of the depth dose distributions has been fitted to determine the mean attenuation coefficient. Calculated $\bar{\mu}$ values are plotted in Fig. 3 for different field sizes.

The electron slowing down spectra have been used to calculate the corresponding stopping power ratio (for details, see 6) of the various photon beam qualities at the calibration depth. The variation of the stopping power ratio as a function of the attenuation property of the beams is shown in Fig. 7 for monoenergetic photons as well as for thin and thick target bremsstrahlung beams. The thick target data pertain to a thickness of one continuous slowing down range (1 r_0) in tungsten and are also fairly representative for beams produced by an intermediate thickness target with a thin flattening filter.

A few examples (4, 10, 20 and 50 MV bremsstrahlung)

are given for the variation of the stopping power ratio with increasing filter thickness (1–8 cm Pb as shown by the symbols for a 1/3 r_o thick tungsten target. It is seen that with increasing target and filter thickness the curve for monoenergetic photons is gradually approached. At first sight this may seem surprising but it can be understood by considering the inserted photon spectra that all give the same $\bar{\mu}_{10}$ for a 10 by 10 cm^2 field (3.5 m^{-1}; 3 MeV monoenergetic, 13 MV thin target and 19 MV thick target photons). Due to the convex shape of the stopping power ratio curve for monoenergetic photons all bremsstrahlung spectra must fall below this curve. Thus, the larger the spectral variance, the lower down will the stopping power ratio fall for a given attenuation coefficient. From the inserted spectra it is seen that this is the case with the thin target with a substantial low energy photon component at the same time as it has many high energy photons. A thick filter will both remove the low and high energy photons and make the stopping power ratio approach the monoenergetic curve.

It is also seen that by plotting the stopping power ratios as a function of the attenuation coefficient the uncertainty in the selection of the stopping power ratio is greatly reduced (cf. Fig. 4 in ref. 6). The stopping power ratio of all filtered clinical photon beams will fall somewhere between the thick target bremsstrahlung and the monoenergetic photon curves. By using this type of plot the correct stopping power ratio within a few tenths of a per cent can be chosen without the need to know the exact target and filter thickness. An even more precise choice is possible if the aproximate filter thickness is known as seen from Fig. 7 and ANDREO & BRAHME (6).

REFERENCES

1. AAPM: A protocol for the determination of absorbed dose from high energy photon and electron beams. Task Group 21, Radiation Therapy Committee of the American Association of Physicists in Medicine. Med. Phys. 10 (1983), 741.
2. ANDREO P.: Monte Carlo simulation of electron transport in water. Absorbed dose and fluence distributions. Report FANZ/-80/3, Dept. of Nuclear Physics, University of Zaragoza, Spain 1980.
3. — Aplicación del método de Monte Carlo a la penetración y dosimetría de haces de electrones. (In Spanish.) Thesis, University of Zaragoza, Spain 1981.
4. — and BRAHME A.: Mean energy in electron beams. Med. Phys. 8 (1981), 682.
5. — — Restricted energy-loss straggling and multiple scattering of electrons in mixed Monte Carlo procedures. Radiat. Res. 100 (1984), 16.
6. — — Stopping power data for high energy photon beams. Phys. Med. Biol. (In press. 1985.)
7. BENTLEY R. E., JONES J. C. and LILLICRAP S. C.: X-ray spectra from accelerators in the range 2 to 6 MeV. Phys. Med. Biol. 12 (1967), 301.
8. BERGER M. J.: Monte Carlo calculation of the penetration and diffusion of fast charged particles. *In:* Methods in computational physics. Vol. 1; Statistical physics. Edited by B. Alder, S. Fernbach and M. Rotenberg. Academic Press, New York 1963.
9. BIGGS P. J. and RUSSELL M. D.: An investigation into the presence of secondary electrons in megavoltage photon beams. Phys. Med. Biol. 28 (1983), 1033.
10. BRAHME A.: Simple relations for the penetration of high energy electron beams in matter. Report SSI: 1975-011, National Institute of Radiation Protection, Stockholm 1975.
11. — Electron transport phenomena and absorbed dose distributions in therapeutic electron beams. Presented at the 14th International Congress of Radiology, Rio de Janeiro 1977.
12. — and SVENSSON H.: Methods of improving dose uniformity in high energy photon and electron beams. Phys. Canada 32 (1976), 28.3.
13. — — Radiation beam characteristics of a 22 MeV microtron. Acta radiol. Oncology 18 (1979), 244.
14. — KRAEPELIEN T. and SVENSSON H.: Electron and photon beams from a 50 MeV racetrack microtron. Acta radiol. Oncology 19 (1980), 305.
15. BROWNRIDGE J., SAMNICK S., STILES P., TIPTON P., VESELKA J. and YEH N.: Determination of the photon spectrum of a clinical accelerator. Med. Phys. 11 (1984), 794.
16. CALZADO A., VANO E., DELGADO V. and GONZALEZ L.: 42 MeV bremsstrahlung spectrum analysis by a photoactivation method. Nucl. Inst. Meth. 225 (1984), 232.
17. GREENING J. R.: Fundamentals of radiation dosimetry. Adam Hilger Ltd., Bristol 1981.
18. HUBBLE J. H.: Photon mass attenuation and energy absorption coefficients from 1 keV to 20 MeV. Int. J. Appl. Radiat. Isot. 33 (1982), 1269.
19. IEC (International Electrotechnical Commission): Medical electron accelerators in the range 1–50 MeV. Section four: performance tolerances. Report 62C (Secretariat) 18, IEC, Geneva 1981.
20. KOCH H. W. and MOTZ J. W.: Bremsstrahlung cross sections formulas and related data. Rev. Mod. Phys. 31 (1959), 920.
21. LEMPERT R. P., JURY J. W. and SHERMAN N. K.: Measurement of bremsstrahlung spectra from 25 MeV electrons on Ta as a function of radiator thickness and emission angle. Nucl. Inst. Meth. 214 (1983), 349.
22. LEUNG P. M., SONTAG M. R., MAHARAJ H. and CHENERY S.: Dose measurements in the build up region for Cobalt 60 therapy units. Med. Phys. 3 (1976), 169.
23. LEVY L. B., WAGGENER R. G., MCDAVID W. D. and PAYNE W. H.: Experimental and calculated bremsstrahlung spectra from a 25 MeV linear accelerator and a 19 MeV betatron. Med. Phys. 1 (1974), 62.
24. — — and WRIGHT A. E.: Measurement of primary bremsstrahlung spectrum from an 8 MeV linear accelerator. Med. Phys. 3 (1976), 173.
25. MATTHEWS J. L. and OWENS R. O.: Accurate formulae for the calculation of high energy electron bremsstrahlung spectra. Nucl. Inst. Meth. 111 (1973), 157.
26. MOHAN R. and CHUI C.: Validity of the concept of separating primary and scatter dose. Med. Phys. 12 (1985), 726.
27. NACP: Recommendations of the Nordic Association of Clinical Physics. Procedures in radiation therapy dosimetry with 5 to 50 MeV electrons and roentgen and gamma rays with maximum photon energies between 1 and 50 MeV. Acta radiol. Ther. Phys. Biol. 11 (1972), 603.
28. — Recommendations of the Nordic Association of Clinical Physics. Procedures in external radiation therapy dosimetry with electron and photon beams with maximum energies between 1 and 50 MeV. Acta radiol. Oncology 19 (1980), 55.
29. NÄFSTADIUS P., BRAHME A. and NORDELL B.: Computer assisted dosimetry of scanned electron and photon beams for radiation therapy. Radiother. and Oncol. 2 (1984), 261.
30. NAHUM A. E.: Calculations of electron flux spectra in water irradiated with megavoltage electron and photon beams with

applications to dosimetry. Thesis, University of Edinburgh. Order No. 77-70006. Xerox University Microfilms, Ann Arbor, Michigan 48106, USA 1976.
31. Nilsson B.: Analysis of quality characteristics of radiotherapeutic photon beams. Thesis, University of Stockholm 1985.
32. — and Brahme A.: Contamination of high energy photon beams by scattered photons. Strahlentherapie 127 (1981), 181.
33. Nordell B. and Brahme A.: Angular distribution and yield from bremsstrahlung targets. Phys. Med. Biol. 29 (1984), 797.
34. Petti P. L., Goodman M. S., Gabriel T. A. and Mohan R.: Investigation of build-up dose from electron contamination of clinical photon beams. Med. Phys. 10 (1983), 18.
35. — — Sisterson J. M., Biggs P. J., Gabriel T. A. and Mohan R.: Sources of electron contamination for the Clinac-35 25 MV photon beam. Med. Phys. 10 (1983), 856.
36. Podgorsak E. B., Rawlinson J. A., Glavinovic M. I. and Johns H. E.: Design of X-ray targets for high energy linear accelerators in radiotherapy. Amer. J. Roentgenol. 121 (1974), 873.
37. Rogers D. W. O. and Bielajew A. F.: The use of EGS for Monte Carlo calculations in medical physics. Report PXNR-2692, National Research Council of Canada, Ottawa 1984.
38. Samuelsson C.: Influence of air cavities on central depth dose curves for 33 MV roentgen rays. Acta radiol. Ther. Phys. Biol. 16 (1977), 465.
39. Schiff L. I.: Energy-angle distributions of thin target bremsstrahlung. Phys. Rev. 83 (1951), 252.
40. SEFM: Procedimientos recomendados para la dosimetría de fotones y electrones de energias comprendidas entre 1 MeV y 50 MeV en radioterapia de haces externos. (In Spanish.) Comité de Dosimetria en Radioterapia de la Sociedad Española de Fisica Medica. Publication No. 1-1984, Madrid 1984.
41. Sternheimer R. M. and Peierls R. F.: General expression for the density effect for the ionization loss of charged particles. Phys. Rev. B3 (1971), 3681.
42. Svensson H. and Brahme A.: Recent advances in electron and photon dosimetry. *In:* Radiation dosimetry. Physical and biological aspects, p. 87. Edited by C. Orton. Plenum Press, New York 1986.
43. Tsai Y. S.: Pair production and bremsstrahlung of charged leptons. Rev. Mod. Phys. 46 (1974), 815.